OPTIMIZATION OF MICRO-CHANNEL HEAT SINK BASED ON GENETIC ALGORITHM AND BACK PROPAGATION NEURAL NETWORK

by

Meixia JIANG [a b] ***and Zhongliang PAN*** [a*]

[a] School of Physics and Telecommunications Engineering, South China Normal University, Guangzhou, China
[b] School of Information Engineering, Guangzhou City Polytechnic, Guangzhou, China

Original scientific paper
https://doi.org/10.2298/TSCI220307121J

In order to efficiently solve the problem of optimization of the micro-channel heat sink, an optimization strategy combining intelligent algorithms and CFD was proposed. The micro-channel heat sink with the trapezoidal cavity and solid/slotted oval pins was proposed to enhance heat transfer. The aspect ratio, distance from the center of the oval pin to the center of the cavity, and slot thickness were design variables. The thermal resistance and pumping power of the micro-channel heat sink were objective functions. Within the selected range of design variables, thirty groups of uniformly sampled sample points were obtained by the Latin hypercube experiment. The 3-D model was established by SOLIDWORKS software, and the numerical simulation was carried out by using FLUENT software. The genetic algorithm optimized back propagation neural network to construct the prediction model, and the simulated data of Latin hypercube sampling were trained to obtain the non-linear mapping relationship between design variables and objective functions. The optimal combination of structural parameters of the micro-channel heat sink was obtained by optimization of the genetic algorithm, which was verified by numerical simulation. The results show that the optimization scheme was suitable for getting the optimal value of the structural parameters of the micro-channel heat sink, which provided a reference for the optimal design of the micro-channel heat sink.

Key words: *micro-channel heat sink, pumping power, thermal resistance, Latin hypercube sampling, GA-BP neural network, genetic algorithm*

Introduction

With the rapid development of microelectronics technology, the power density of electronic devices is increasing, which poses a significant challenge to the thermal management of 3-D integrated circuits [1, 2]. The micro-channel heat sink has good heat transfer performance, so it is widely used in heat dissipation design of electronic devices, such as micro fins, micro pits, micro ribs and so on [3-7]. The results show that these heat transfer structures not only enhance the heat transfer performance but also increase the pumping power. In order to reduce the increase of pumping power and improve heat transfer performance, Steinke *et al*. [8] and Kuppusamy *et al*. [9] proposed a micro-channel heat sink with secondary flows, which enhances the heat transfer performance with minor pumping power and thermal resistance. Lin

* Corresponding author, e-mail: panzhongliang@m.scnu.edu.cn

et al. [10] suggested the wavy micro-channel heat sink with changing wavelength or/and amplitude along the flow direction can reduce thermal resistance and pumping power. Fan *et al.* [11] studied a novel cylindrical oblique fin micro-channel heat sink, and the results show that the heat transfer performance of the cylindrical oblique fin micro-channel heat sink over conventional straight fin mini channel heat sink. Rajabi *et al.* [12] studied the effect of the micro-channel heat sink with sectional oblique fins on heat transfer and flow streamline distribution. Chuan *et al.* [13] proposed solid fins instead of porous fins to reduce the pressure drop of the micro-channel heat sink. It can be seen from the literature that the micro-channel heat sink with a secondary flow channel can significantly improve the heat transfer effect.

Good design of micro-channel heat sink structure can effectively improve heat transfer performance. In engineering applications, geometric structure parameters of the micro-channel heat sink can be effectively optimized by numerical calculation methods to improve heat transfer performance and reduce pumping power. Shi *et al.* [14] studied the optimization of a single-layer nanofluid-cooled micro-channel heat sink with a rectangular cross-section based on a multi-objective to get minimize the thermal resistance and pumping power of the micro-channel heat sink. Ansari *et al.* [15] performed optimization of the micro-channel heat sink with a grooved structure by a multi-objective evolutionary algorithm. Xia *et al.* [16] combined the multi-objective evolutionary algorithm (MOEA) with CFD to optimize the geometry of micro-channel heat sink with arc-shaped grooves and ribs.

Genetic algorithm (GA) and back propagation (BP) neutral network were widely applied in certain engineering fields, such as the shape design of drones, automobile structure optimization and so on, but it is less in the optimization design of micro-channel heat sink. Han *et al.* [17] took the shape design of drones as the research object. The hybrid GA-BP model was constructed by optimizing BP neural network with the GA to evaluate and screen out scientific design schemes effectively. Zhang *et al.* [18] proposed a BP neural network optimization method based on the GA to speed the training of BP neural network to overcome BP neural network disadvantage of being easily stuck in a local minimum. Tam *et al.* [19] applied the hybrid model including BP neural network and GA to estimate the nanofluids density. Rahimi *et al.* [20] used ANN and GA to predicate the flow characteristic in serpentine micro-channels. Therefore, this paper studied GA optimized the BP neural network to construct a GA-BP neural network model, overcome the local optimization problem of BP neural network, and improved the training efficiency of neural network on thermal resistance and pump power, it has certain novelty in the application of the optimization of the micro-channel heat sink.

In this paper, the micro-channel heat sink with trapezoidal cavity and solid/slotted oval pins was studied, the aspect ratio, *AR*, distance from the center of the oval pin to the center of the cavity, *X*, and slot thickness, *t*, were design variables. The thermal resistance and pumping power of the micro-channel heat sink were objective functions. Latin hypercube sampling was designed, and the numerical simulation was carried out by using the FLUENT software. The GA optimized the BP neural network to construct a GA-BP neural network model with high accuracy. Then the GA was used for global optimization to obtain the optimal combination of parameters of the micro-channel heat sink so that the thermal resistance and pumping power of the micro-channel heat sink reach optimal, respectively. It provides an essential reference for the structural parameter design of the micro-channel heat sink with better comprehensive heat transfer performance.

Micro-channel heat sink model

Micro-channel heat sink structure and description

Alfellag *et al.* [21] proposed the micro-channel heat sink with trapezoidal cavity and solid/slotted oval pins as the reference design channel and optimized its structural parameters. The schematic diagram and geometrical parameters of the present study are illustrated in figs. 1(a)-1(c). The geometric parameters of the micro-channel heat sink are shown in tab. 1. The overall structure of the micro-channel is shown in fig. 1(a). The length, L_s, height, H_s, and width, W_s of the computational domain are 10 mm, 0.35 mm, and 0.3 mm, respectively, corresponding to that proposed by [21], as shown in fig. 1(b). The height, h_s, and width, W_c, of a single micro-channel heat sink are 0.2 mm and 0.1 mm, respectively, corresponding to that proposed by [21], as shown in figs. 1(b) and 1(c). The single micro-channel heat sink has two cavities and two oval pins along the axial direction of the flow. The top of the cavity length, *a*, bottom length, *b*, and height, *c*, are 0.2 mm, 0.1 mm, and 0.08 mm, respectively, corresponding to that proposed by [21], as shown in fig. 1(c). The small diameter, *d*, of the oval pins remains constant at 0.04 mm, while the large diameter, *D*, is changeable based on the *AR*, which is defined as *D*/*d*. The *AR* changes in the range of 1.25-2.75. The distance from the micro-channel heat sink entrance to the cavity center, *s*, is 3 mm, while the distance between the two-cavity centers, *r*, is 4 mm, corresponding to that proposed by [21], as shown in fig. 1(b). The two inclined grooves on the oval pin are used with a tilt angle of 8° with the axial direction, as shown in fig. 1(c). The slot thickness, *t*, is changed in the range of 0.008-0.015 mm. The distance from the center of the oval pin to the center of the cavity is defined as *X*, which changes in the range of 0-0.006 mm. In the paper, the substrate of the micro-channel heat sink is made of aluminum, and the constant wall heat flux, which is 1000 kW/m^2, was supplied to the base bottom. The fluid is water. The inlet speed and temperature are 8 m/s and 300 K.

Table 1. Geometric parameters of the micro-channel heat sink

Parameters	Value [mm]	Parameters	Value [mm]	Parameters	Value [mm]
H_s	0.35	*S*	3	*d*	0.04
W_s	0.3	*R*	4	*X*	0-0.06
L_s	10	*A*	0.2	$W_{f/2}$	0.1
h_s	0.2	*B*	0.1	*D*	0.05-0.11
W_c	0.1	*C*	0.08	*T*	0.008-0.015

Model calculation and processing

In order to simplify the problem, the following assumptions are considered for heat transfer and fluid flow characteristics in the micro-channel heat sink: cooling fluid is steady laminar flow, and the fluid is incompressible and single-phase flow. The thermophysical properties of fluids and solids do not change with temperature. The effects of gravity, buoyancy and thermal radiation are ignored. Based on the assumptions, the flow and heat transfer process of fluid should follow certain conservation equations, which governing equations are [1]:

$$\nabla \vec{u} = 0 \tag{1}$$

$$\rho(\vec{u}\nabla)\vec{u} = -\nabla P + \mu\nabla^2\vec{u} \tag{2}$$

$$\rho c_p \vec{u}(\nabla T) = \nabla(\lambda_f \nabla T) \tag{3}$$

where $\vec{u}$ is the velocity matrix, P – the pressure, T – the temperature, ρ – the fluid density, μ – the viscosity, λ_f – the thermal conductivity of the fluid, and c_p – the specific heat of coolant.

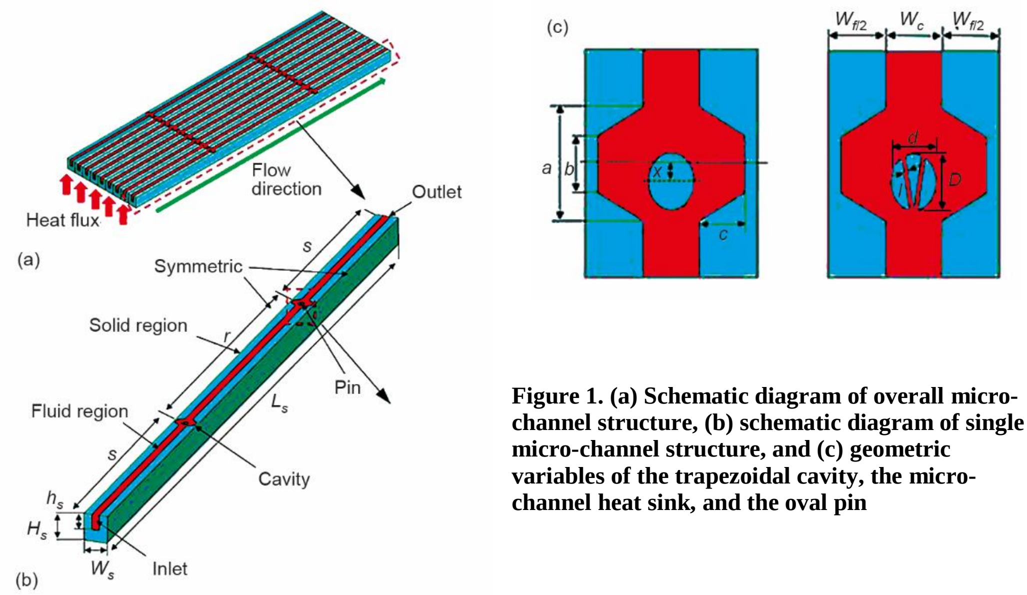

Figure 1. (a) Schematic diagram of overall micro-channel structure, (b) schematic diagram of single micro-channel structure, and (c) geometric variables of the trapezoidal cavity, the micro-channel heat sink, and the oval pin

For the solid substrate, the energy equations can be expressed:

$$\lambda_s \nabla^2 T = 0 \tag{4}$$

where λ_s is the thermal conductivity of the solid.

The CFD simulation analysis was carried out for the micro-channel heat sink by varying oval pin parameters such as X, AR, and t. Using single-phase liquid water as coolant. The whole solution process was a steady-state. The SIMPLE algorithm was used to deal with the pressure-velocity coupling. Convergence criteria scaled residuals for continuity, momentum, and energy equations are less 10^{-4}, 10^{-5}, and 10^{-6}, respectively.

Grid independence test

For the micro-channel heat sink with the trapezoidal cavity and solid/slotted oval pin, the tetrahedral grid was used to divide, as shown in fig. 2. A non-uniform grid was used for the oval pin. The effect of the grid density on the computational results is evaluated by simulating six different grid numbers, when X, AR, and t are 0.039 mm, 1.675, and 0.013 mm, respectively, and the inlet speed is 8 m/s. The highest value of Reynolds number at the inlet of the micro-channel in the current study is 1200. The comparison results of six different grid numbers are shown in tab. 2. The percentage error for pressure drop and maximum temperature between the mesh numbers of 1964170 and 3928340 was less than 0.17% and 0.05%, respectively. Therefore, the mesh numbers of 1964170 were adopted for simulation analysis in the current study to save the number of grids and computational time.

Table 2. Meshing contrast

Number of elements	T_{max} [K]	ΔP [KPa]	T_{max} error [%]	ΔP error [%]
654723	316.69	314.29	0.25	3.03
982085	317.03	309.53	0.15	1.46
1964170	317.49	305.06	criterion	
2455212	317.56	304.74	0.02	0.10
2805957	317.62	304.61	0.04	0.15
3928340	317.66	304.53	0.05	0.17

Genetic algorithm optimized back propagation neural network prediction model formation

Latin hypercube sampling

Latin hypercube sampling (LHS) is a random sampling experimental design method, which was proposed by McKay *et al.* [22]. It can select a group of sample points by sampling in the space, so that the obtained sample points can be evenly distributed in the area. In order to get the non-linear mapping relationship between design variables and objective functions, it is necessary to conduct an experimental design. The design of LHS can make sample points evenly distributed in the sampling interval and provide a high-precision original database for GA-BP neural network model training. The design variables are X, t, and AR, which change in the range of 0-0.06 mm, 0.008-0.015 mm, and 1.25-2.75, respectively. Thirty groups of sample points were evenly selected within the scope of the design variables. The distribution of LHS sampling points is shown in fig. 3. The parameters combination of thirty groups of sample points was numerically simulated by FLUENT software to establish the original database of the GA-BP neural network, as shown in tab. 3.

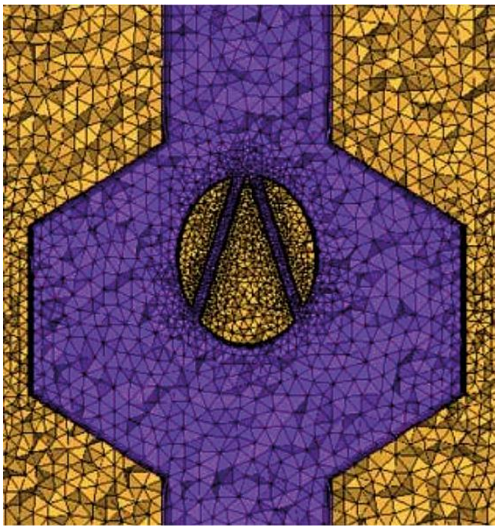

Figure 2. Meshing of the micro-channel heat sink with cavity and pin

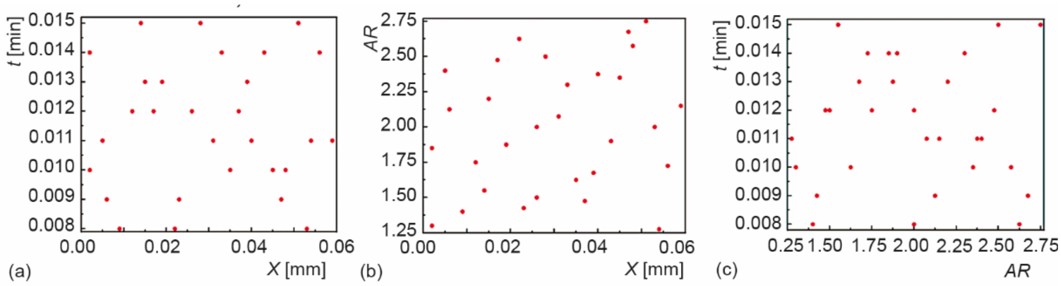

Figure 3. Distribution of Latin hypercube sampling points in sampling space; (a) *X-t*, (b) *X-AR*, and (c) *AR-t*

Table 3. Latin hypercube sampling points and numerical simulation results

Case no.	X [mm]	AR	t [mm]	R_t [KW^{-1}]	P_p [W]
1	0.040	2.375	0.011	5.5500	$9.1523 \cdot 10^{-4}$
2	0.005	2.400	0.011	5.7500	$6.2196 \cdot 10^{-4}$
3	0.048	2.575	0.010	5.4367	$1.2075 \cdot 10^{-3}$
4	0.009	1.400	0.008	5.8933	$5.1876 \cdot 10^{-4}$
5	0.017	2.475	0.012	5.6933	$6.8889 \cdot 10^{-4}$
6	0.023	1.425	0.009	5.9200	$5.3726 \cdot 10^{-4}$
7	0.028	2.500	0.015	5.6867	$7.0983 \cdot 10^{-4}$
8	0.043	1.900	0.014	5.7133	$6.8330 \cdot 10^{-4}$
9	0.047	2.675	0.009	5.4033	$1.3184 \cdot 10^{-3}$
10	0.053	2.000	0.008	5.4500	$1.1186 \cdot 10^{-3}$
11	0.022	2.625	0.008	5.5733	$8.7991 \cdot 10^{-4}$
12	0.039	1.675	0.013	5.8300	$6.1012 \cdot 10^{-4}$
13	0.035	1.625	0.010	5.7567	$6.0787 \cdot 10^{-4}$
14	0.019	1.875	0.013	5.8800	$5.5302 \cdot 10^{-4}$
15	0.051	2.750	0.015	5.5967	$9.6957 \cdot 10^{-4}$
16	0.031	2.075	0.011	5.6767	$6.9080 \cdot 10^{-4}$
17	0.056	1.725	0.014	5.7233	$7.6200 \cdot 10^{-4}$
18	0.002	1.850	0.014	5.8900	$5.3173 \cdot 10^{-4}$
19	0.026	1.500	0.012	5.9000	$5.3702 \cdot 10^{-4}$
20	0.026	2.000	0.012	5.7633	$6.1494 \cdot 10^{-4}$
21	0.037	1.475	0.012	5.8567	$5.7301 \cdot 10^{-4}$
22	0.054	1.275	0.011	5.8133	$6.7042 \cdot 10^{-4}$
23	0.014	1.550	0.015	6.0433	$5.1228 \cdot 10^{-4}$
24	0.045	2.350	0.010	5.5100	$1.0341 \cdot 10^{-3}$
25	0.059	2.150	0.011	5.4633	$1.1324 \cdot 10^{-3}$
26	0.012	1.750	0.012	5.9067	$5.3150 \cdot 10^{-4}$
27	0.002	1.300	0.010	5.9800	$5.1531 \cdot 10^{-4}$
28	0.006	2.125	0.009	5.7567	$5.7210 \cdot 10^{-4}$
29	0.015	2.200	0.013	5.7967	$5.9428 \cdot 10^{-4}$
30	0.033	2.300	0.014	5.6933	$7.1539 \cdot 10^{-4}$

Genetic algorithm optimized back propagation neural network model establishing and training

The BP neural network is a multilayer feed-forward network trained by an error BP algorithm. It is widely used in engineering to deal with non-linear and complex systems. It can be tacking non-linearity and mapping input-output information [23]. The network structure is composed of the input layer, hidden layer, and output layer. Layers are connected by weights. The neurons in layers are not connected. The weight and threshold of the BP neural network have a significant influence on the prediction accuracy of the neural networks. In order to reduce the prediction error of the BP neural network and improve the operation speed of the BP neural network, the BP neural network was optimized by a GA to establish the GA-BP neural network model.

The GA-BP neural network has three parts: BP neural network, GA optimizes weights and thresholds, and BP neural network prediction. In this paper, the GA-BP neural network was used to solve the optimization problem. The BP neural network model is shown in fig. 4. The input layer has three nodes, which were X, AR, and t, respectively. The number of hidden layers was 5. The output layer had two nodes, which were R_t and P_p. The flow chart about the GA-BP neural network algorithm was shown in fig. 5. The mean square error function which was trained by BP neural network was used for the fitness function of the genetic algorithm. The initial population number was 35, the maximum iteration number was 100, the crossover probability was 0.3, and the mutation probability was 0.2.

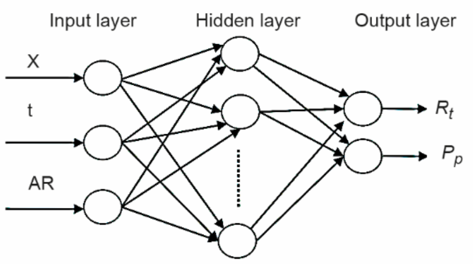

Figure 4. The BP neural network model

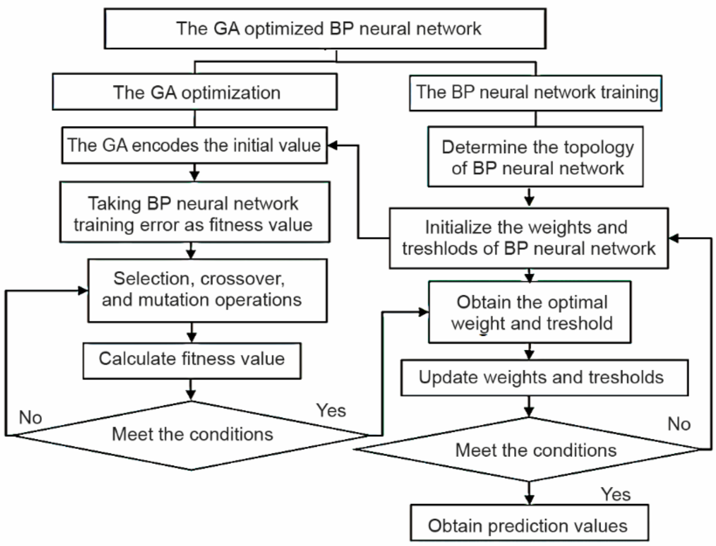

Figure 5. The GA optimized BP neural network algorithm flow

Twenty-two groups data were selected as network training samples, and the remaining eight groups data were used as test samples to test the accuracy of the GA-BP neural network model. In network training, the parameters of the GA-BP neural network are shown in tab. 4. The learning rate is 0.1, training times are 100, and training objectives are 0.00001. Trainlm is the training function, Tansig is the hidden layer transfer function, and Purelin is the output layer transfer function. Mean square error (MSE) is the performance function. In order to ensure the precision of network training, the input and output data are normalized and denormalized by the normalized function mapminmax of MATLAB software, which is defined:

$$y^* = \frac{y - y_{\min}}{y_{\max} - y_{\min}} \tag{5}$$

where y and y^* are the values before and after normalization, respectively. $y_{\min}$ and $y_{\max}$ are minimum and maximum values in the sample data, respectively.

Table 4. Parameters of GA optimized BP neural network

Parameters	Value	Parameters	Value
Learning rate	0.1	Training function	Trainlm
Training times	100	Hidden layer transfer function	Tansig
Training objectives	0.00001	Output layer transfer function	Purelin
Performance function	Mean square error (MSE)		

The output of expected values and predicted values about the BP neural network and GA-BP neural network is shown in fig. 6. The results show that the GA-BP neural network is better than BP neural network in predicting R_t and P_p. The data comparison between expected and predicted values of R_t and P_p is shown in tab. 5. In order to accurately analyze the value of the prediction error, the relative errors, E_r, of R_t, and P_p are calculated by:

$$E_\mathrm{r} = \frac{|m-n|}{n}100\% \tag{6}$$

where m and n are predicted values and expected values, respectively.

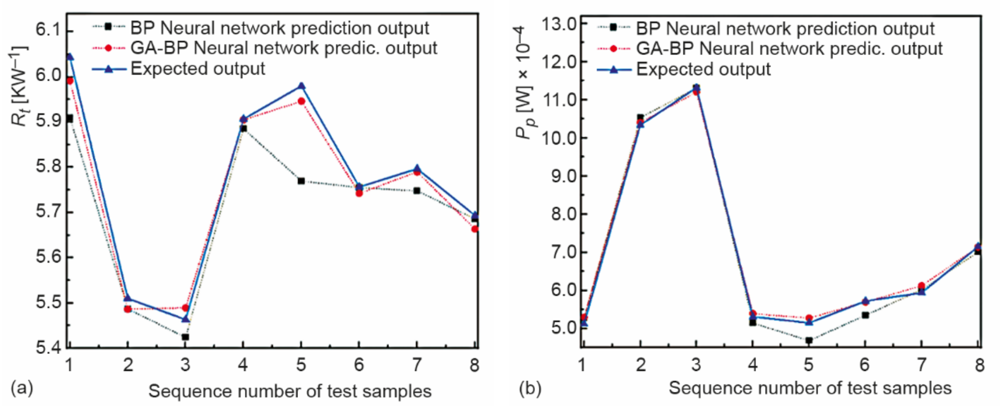

Figure 6. Expected and predicted values output of BP neural network and GA optimized BP neural network; (a) thermal resistance and (b) pumping power

Table 5. Data comparison between expected and predicted values

Case no.	R_t [KW^{-1}]			P_p [W]		
	BP predicted	GA-BP predicted	Expected	BP predicted	GA-BP predicted	Expected
23	5.9100	5.9916	6.0433	$5.2737 \cdot 10^{-4}$	$5.2982 \cdot 10^{-4}$	$5.1200 \cdot 10^{-4}$
24	5.4870	5.4862	5.5100	$1.0533 \cdot 10^{-3}$	$1.0405 \cdot 10^{-3}$	$1.0340 \cdot 10^{-3}$
25	5.4239	5.4893	5.4633	$1.1310 \cdot 10^{-3}$	$1.1206 \cdot 10^{-3}$	$1.1320 \cdot 10^{-3}$
26	5.8854	5.9051	5.9067	$5.1440 \cdot 10^{-4}$	$5.3928 \cdot 10^{-4}$	$5.3100 \cdot 10^{-4}$
27	5.7697	5.9464	5.9800	$4.6856 \cdot 10^{-4}$	$5.2752 \cdot 10^{-4}$	$5.1500 \cdot 10^{-4}$
28	5.7551	5.7426	5.7567	$5.3491 \cdot 10^{-4}$	$5.6973 \cdot 10^{-4}$	$5.7200 \cdot 10^{-4}$
29	5.7481	5.7898	5.7967	$6.0237 \cdot 10^{-4}$	$6.1257 \cdot 10^{-4}$	$5.9400 \cdot 10^{-4}$
30	5.6861	5.6636	5.6933	$7.0072 \cdot 10^{-4}$	$7.1384 \cdot 10^{-4}$	$7.1500 \cdot 10^{-4}$

The relative errors between expected values and predicted values about thermal resistance of BP neural network and GA-BP neural network are 0.028%-3.517% and 0.027%-0.855%, respectively, as shown in fig. 7(a). The relative errors between expected values and predicted values about pumping power of the BP neural network and GA-BP neural network are 0.088%-9.017% and 0.162%-3.480%, respectively, as shown in fig. 7(b). The results show that GA-BP neural network has more accurate prediction output and high fitting degree, which effectively improves the prediction ability. The GA-BP neural network model can be used to reflect the complex nonlinear mapping relationship between the structural parameters of the micro-channel heat sink and objective functions. It has certain accuracy and generalization, and can be applied to predicting thermal resistance and pumping power of the micro-channel heat sink.

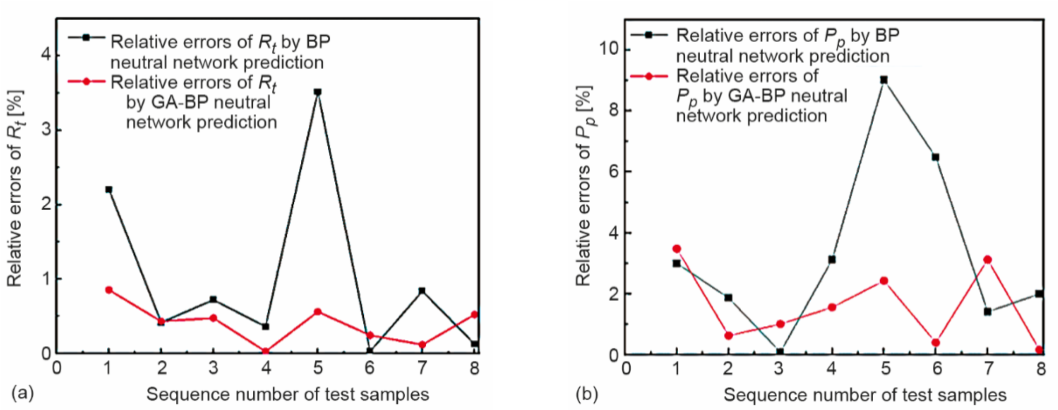

Figure 7. Relative errors between expected and predicted values output of BP neural network and GA optimized BP neural network; (a) thermal resistance and (b) pumping power

Objective function optimization based on genetic algorithm

Thermal resistance and pumping power are two important indexes to evaluate the performance of the micro-channel heat sink. Therefore, the thermal resistance and pumping work are established as the objective functions, which are defined:

$$R_t = \frac{T_{\mathrm{s,max}} - T_{\mathrm{f,in}}}{qA_{\mathrm{s}}} \tag{7}$$

$$P_p = uNA_{\mathrm{ch}}\Delta P \tag{8}$$

where $T_{\mathrm{s,max}}$, $T_{\mathrm{f,in}}$, u, A_{s} are maximum temperature, inlet temperature, inlet velocity, and bottom area of the micro-channel heat sink, respectively, q – the heat flow density, A_{ch} – the cross-sectional area of a single micro-channel heat sink, N – the total number of the micro-channel, ΔP – the pressure drop of micro-channels, which is defined:

$$\Delta P = P_{\mathrm{in}} - P_{\mathrm{out}} \tag{9}$$

where P_{in} and P_{out} are the pressure at the inlet and outlet of the micro-channel heat sink, respectively.

The mathematical model of the optimization problem is described:

$$\min f_1(X, AR, t) = \min[R_{\mathrm{t}}\ (X, AR, t)] \tag{10}$$

$$\min f_2(X, AR, t) = \min[P_{\mathrm{p}}(X, AR, t)] \tag{11}$$

s.t.

$$0 < X < 0.06$$

$$1.25 < AR < 2.75$$

$$0.008 < t < 0.015$$

The Reynolds number is defined:

$$\mathrm{Re} = \frac{\rho u_{\mathrm{m}} D_{\mathrm{h}}}{\mu_{\mathrm{f}}} \tag{12}$$

where u_{m} is the fluid velocity and D_{h} is the hydraulic diameter of the micro-channel:

$$D_{\mathrm{h}} = 2\frac{h_{\mathrm{s}} W_c}{h_{\mathrm{s}} + W_c} \tag{13}$$

The thermal resistance and pumping work are predicted by GA-BP neural network, and the prediction results are taken as the individual fitness of the GA. Then the objective functions are optimized by selection, crossover, and mutation to obtain the objective functions optimum solution and structure parameters of the micro-channel heat sink corresponding to the optimal solution. In the GA, the initial population number is 10, the maximum iteration number is 40, the crossover probability is 0.3, and the mutation probability is 0.1. The global optimization fitness curve of the GA is shown in fig. 8. The results show that after 40 iterations of optimization, the thermal resistance fitness value converges to 5.38 K/W, and the pumping power fitness value converges to $4.96 \cdot 10^{-4}$ W.

Results and discussions

The comparison between the predicted and numerical simulation verification values of corresponding structural parameters after optimization are shown in tabs. 6 and 7. When X is 0.056 mm, AR is 2.447, and t is 0.009 mm, the predicted value and numerical simulation

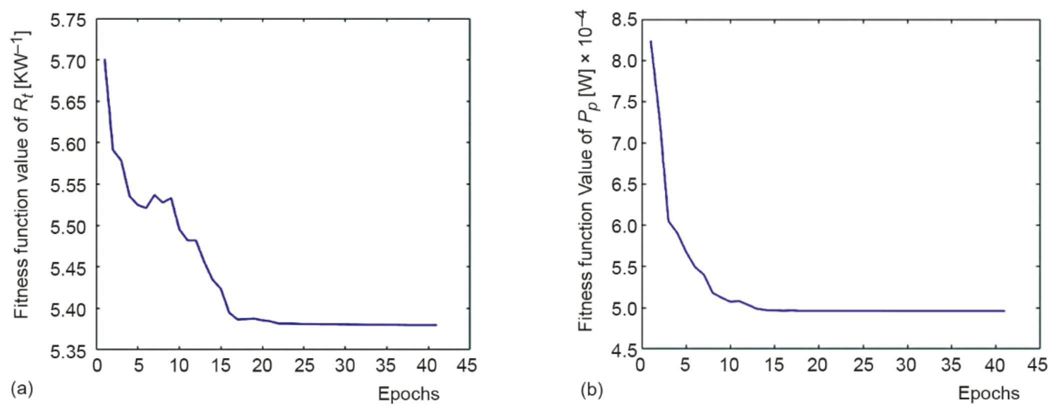

Figure 8. Global optimization fitness curve of GA; (a) thermal resistance fitness curve, (b) pumping power fitness curve

verification value of the thermal resistance are 5.38 K/W and 5.02 K/W, respectively, and the relative error is 6.69%. When *X* is 0.003 mm, *AR* is 1.254, and *t* is 0.013 mm, the predicted value and numerical simulation verification value of pumping power are $4.96 \cdot 10^{-4}$ W and $5.19 \cdot 10^{-4}$ W, respectively, and the relative error is 4.43%. It is shown that the GA-BP neural network proposed in this paper has high precision prediction performance.

Table 6. Optimization results of thermal resistance based on GA and numerical simulation verification

Parameters	*X* [mm]	*AR*	*t* [mm]	Predicted value [KW^{-1}]	Numerical simulation [KW^{-1}]	Relative error [%]
Value	0.056	2.447	0.009	5.38	5.02	6.69

Table 7. Optimization results of pumping power based on GA and numerical simulation verification

Parameters	*X* [mm]	*AR*	*t* [mm]	Predicted value [W]	Numerical simulation [W]	Relative error [%]
Value	0.003	1.254	0.013	4.96E-04	5.19E-04	4.43

Comparison and verification of CFD simulation experiment results are shown in tabs. 8 and 9. It compared three different cases. They were before optimization, after optimization, and Alfellag's design [21], respectively. The results showed that the thermal resistance of the simulation results after optimization was reduced by 13.89% and 9.55%, respectively, compared with that before optimization and Alfellag's design. The pumping power of the simulation results after optimization was reduced by 14.92% and 8.63%, respectively, compared with that before optimization and Alfellag's design. The results show that the thermal resistance and pumping power of the micro-channel heat sink can be optimized by GA-BP neural network, respectively.

The friction coefficient can reflect the resistance of the micro-channel to fluid-flow. The greater the friction coefficient, the greater the fluid resistance of the micro-channel, and vice versa. Nusselt number can reflect the intensity of convective heat transfer. The larger the Nusselt number, the stronger the convective heat transfer intensity of the micro-channel, and vice versa. In order to evaluate the heat transfer performance of the optimized micro-channel

Table 8. Comparison between optimization results and numerical simulation about thermal resistance

Case	X [mm]	AR	t [mm]	T [K]	T [°C]	R_t [KW^{-1}]
Before optimization	0.039	1.675	0.013	317.490	44.340	5.83
After optimization	0.056	2.447	0.009	315.046	41.896	5.02
Alfellag's design	0.030	1.250	0.008	316.662	43.512	5.55

Table 9. Comparison between optimization results and numerical simulation about pumping power

Case	X [mm]	AR	t [mm]	Δp [KPa]	P_p [W]
Before optimization	0.039	1.675	0.013	305.058	$6.10\cdot10^{-4}$
After optimization	0.003	1.254	0.013	259.741	$5.19\cdot10^{-4}$
Alfellag's design	0.030	1.250	0.008	283.792	$5.68\cdot10^{-4}$

heat sink, the friction factor and Nusselt number are used to evaluate the intensity of convective heat transfer and flow resistance of the optimized micro-channel heat sink, respectively, which are defined in eqs. (14)-(16) [21]:

$$\mathrm{Nu} = \frac{hD_\mathrm{h}}{\lambda_\mathrm{f}} \tag{14}$$

$$h = \frac{Q}{NA_\mathrm{ch}\Delta T} = \frac{qA_\mathrm{s}}{NA_\mathrm{ch}(T_\mathrm{s} - T_\mathrm{f})} \tag{15}$$

$$f = \frac{2\Delta p D_\mathrm{h}}{\rho L_\mathrm{s} U_\mathrm{in}^2} \tag{16}$$

where Nu, D_h, and h are Nussert number, the hydraulic diameter of the micro-channel, and convective heat transfer coefficient, respectively. While T_s, T_f, and f are the average temperature of the heated bottom, the average temperature of the fluid, and the friction factor of the micro-channel heat sink.

The nephogram of the temperature field for three different cases is shown in fig. 9. Compared with the before optimization and Alfellag's design, the maximum temperature of the micro-channel heat sink after optimization is reduced by 5.51% and 3.71%, respectively. The ratio of Nussert number of the micro-channel heat sink after optimization to that before optimization was 1.09. The ratio of Nussert number of the micro-channel after optimization to that Alfellag's design was 1.10. It shows that the heat transfer performance of the micro-channel heat sink after optimization (X = 0.056 mm, AR = 2.447, and t = 0.009 mm) was improved. The nephogram of the pressure distribution for three different cases is shown in fig. 10. Compared with the before optimization and Alfellag's design, the pressure drop of the micro-channel heat sink after optimization is reduced by 14.86% and 8.47%, respectively. The ratio of the friction factor of micro-channel heat sink after optimization to that before optimization was 0.73. The ratio of the friction factor of the micro-channel after optimization to that Alfellag's design was 0.79. It shows that the friction factor of the micro-channel heat sink after optimization (X = 0.003 mm, AR = 1.254, and t = 0.013 mm) was reduced. The results show that GA-BP neural network can be effectively applied to the optimal design of micro-channel heat sink.

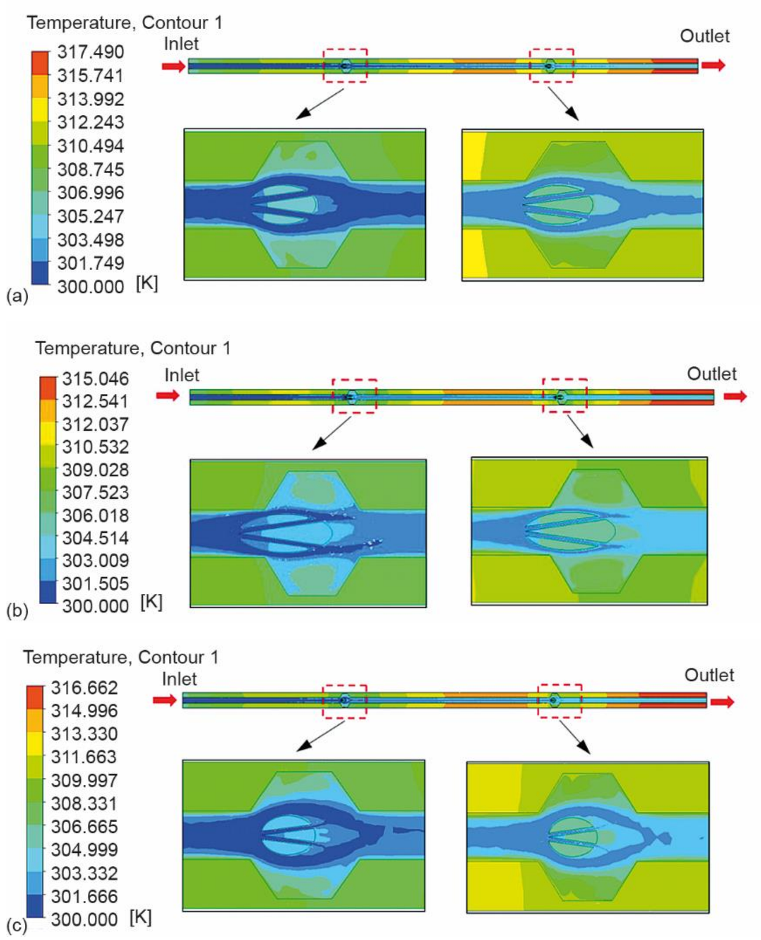

Figure 9. Nephogram of temperature field; (a) before optimization, (b) after optimization, and (c) Alfellag's design

Conclusions

This paper takes the micro-channel heat sink with the trapezoidal cavity and solid/slotted oval pins as studied. It presents an optimization strategy combining intelligent algorithm (GA-BP neural network) and CFD. The thermal resistance and pumping power were chosen as objective functions. The experiment results show that the GA-BP neural network has high prediction accuracy for the resistance and pumping power of the micro-channel heat sink. The GA was used for global optimization to obtain the optimal combination of parameters of the micro-channel heat sink, so that the thermal resistance and pumping power of the micro-channel heat sink can reach optimal, respectively. Hence, optimizing the micro- channel heat sink based on GA and BP neural network can improve the heat transfer performance of the micro-channel heat sink. This optimization method provides the engineering reference for the optimization design of structural parameters of the micro-channel heat sink.

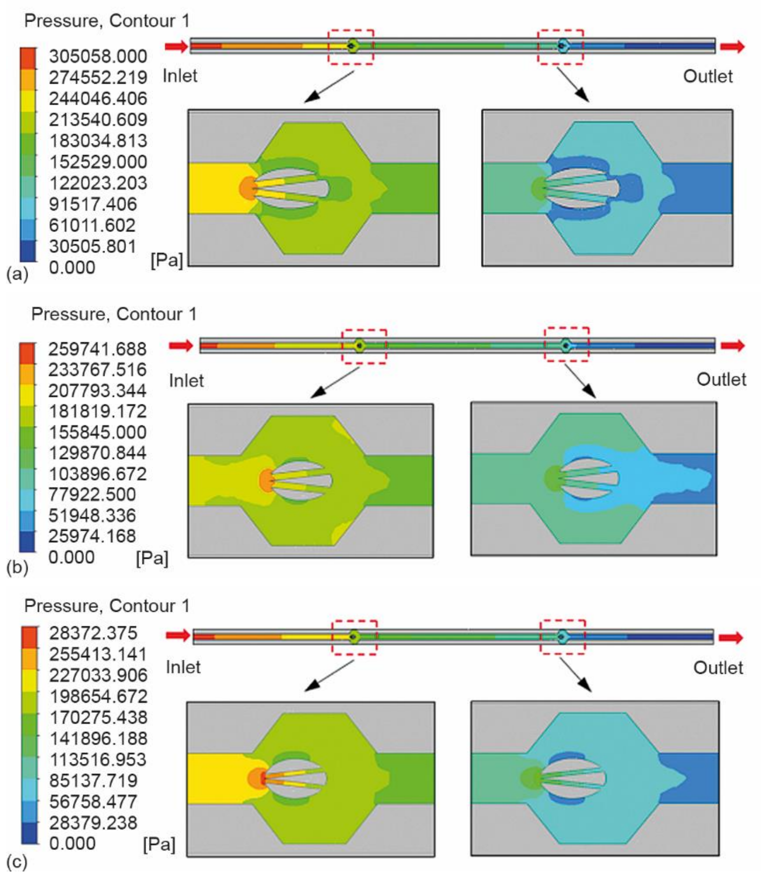

Figure 10. Nephogram of pressure distribution; (a) before optimization, (b) after optimization, and (c) Alfellag's design
(*for color image see journal web site*)

Acknowledgment

This work was supported by Guangzhou Science and Technology Project (201904010107), Guangdong Provincial Natural Science Foundation of China (2019A1515010793), Guangdong Province Science and Technology Project (2016B090918071).

References

[1] Wang, T. H., *et al*., Optimization of a Double-Layered Micro-channel Heat Sink with Semi-Porous-Ribs by Multi-Objective Genetic Algorithm, *International Journal of Heat & Mass Transfer*, *149* (2020), Mar., ID 119217
[2] Zeng, S., *et al*., Thermohydraulic Analysis of a New Fin Pattern Derived from Topology Optimized Heat Sink Structures, *International Journal of Heat & Mass Transfer*, *147* (2020), Feb., 118909
[3] Vinoth, R., Senthil, K. D., Numerical Study of Inlet Cross-section Effect on Oblique Finned Micro-channel Heat Sink, *Thermal Science*, *22* (2018), 6, pp. 2747-2757
[4] Shamsi, M. R., *et al*., Increasing Heat Transfer of Non-Newtonian Nanofluid in Rectangular Micro-channel with Triangular Ribs, *Physica E-Low-Dimensional Systems & Nanostructures*, *93* (2017), Sept., pp. 167-178

[5] Heydari, A., *et al*., The Effect of Attack Angle of Triangular Ribs on Heat Transfer of Nanofluids in a Micro-channel, *Journal of Thermal Analysis and Calorimetry*, *131* (2018), 3, pp. 2893-2912
[6] Chai, L., *et al*., Thermohydraulic Performance of Micro-channel Heat Sinks with Triangular Ribs on Sidewalls-Part 2: Average Fluid Flow and Heat Transfer Characteristics, *International Journal of Heat and Mass Transfer*, *128* (2019), Jan., pp. 634-648
[7] Shi, X. J., *et al*., Geometry Parameters Optimization for a Micro-channel Heat Sink with Secondary Flow Channel, *International Communications in Heat & Mass Transfer*, *104* (2019), May, pp. 89-100
[8] Steinke, M. E., Kandlikar, S. G., Single-Phase Heat Transfer Enhancement Techniques in Micro-channel and Minichannel Flows, *Proceedings,* International Conference on Micro-channels and Mini-Channels, Rochester, N. Y., USA, 2004
[9] Kuppusamy, N. R., *et al*., Numerical Study of Thermal Enhancement in Micro-channel Heat Sink with Secondary Flow, *International Journal of Heat and Mass Transfer*, *78* (2014), Nov., pp. 216-223
[10] Lin, L., *et al*., Heat Transfer Enhancement in Micro-channel Heat Sink by Wavy Channel with Changing Wavelength/Amplitude, *International Journal of Thermal Sciences*, *118* (2017), Aug., pp. 423-434
[11] Fan, Y., *et al*., A Simulation and Experimental Study of Fluid Flow and Heat Transfer on Cylindrical Oblique-Finned Heat Sink, *International Journal of Heat and Mass Transfer*, *61* (2013), June, pp. 62-72
[12] Rajabi, F. B., *et al*., Effects of Pin Tip-Clearance on the Performance of an Enhanced Micro-channel Heat Sink with Oblique Fins and Phase Change Material Slurry, *International Journal of Heat and Mass Transfer*, *83* (2015), Apr., pp. 136-145
[13] Chuan, L., *et al*., Fluid Flow and Heat Transfer in Micro-channel Heat Sink Based on Porous Fin Design Concept, *International Communications in Heat & Mass Transfer*, *65* (2015), July, pp. 52-57
[14] Shi, X. J., *et al*., Multi-objective Optimization on the Geometrical Parameters of a Nanofluid-Cooled Rectangular Micro-channel Heat Sink (in Chinese), *Journal of Xi'an Jiaotong University*, *52* (2018), 5, pp. 56-61
[15] Ansari, D., *et al*., Multi-objective Optimization of a Grooved Micro-channel Heat Sink, *Components and Packaging Technologies, IEEE Transactions on*, *33* (2010), 4, pp. 767-776
[16] Xia, G. D., *et al*., Numerical Simulation and Multi-objective Optimization of a Micro-channel Heat Sink with Arc-Shaped Grooves and Ribs, *Numerical Heat Transfer*; *Part A: Applications*, *70* (2016), 9, pp. 1041-1055
[17] Han, J. X., *et al*., Product Modeling Design Based on Genetic Algorithm and BP Neural Network, *Neural Computing and Applications*, *33* (2021), 9, pp. 4111-4117
[18] Zhang, Y. X., *et al*., Weld Appearance Prediction with BP Neural Network Improved by Genetic Algorithm During Disk Laser Welding, *Journal of Manufacturing Systems*, *34* (2015), Jan., pp. 53-59
[19] Tam, B. N, Hiroshi, H., Training Artificial Neural Network Using Modification of Differential Evolution Algorithm, *International Journal of Machine Learning and Computing*, *5* (2015), 1, pp. 1-6
[20] Rahimi, M., *et al*., Application of Artificial Neural Network and Genetic Algorithm Approaches for Prediction of Flow Characteristic in Serpentine Micro-channels, *Chemical Engineering Research & Design: Transactions of the Institution of Chemical Engineers Part A, 98* (2015), June, pp. 147-156
[21] Alfellag, M. A., *et al*., Optimal Hydrothermal Design of Micro-channel Heat Sink Using Trapezoidal Cavities and Solid/Slotted Oval Pins, *Applied Thermal Engineering*, *158* (2019), July, 113765
[22] McKay, M. D., *et al*., A Comparison of Three Methods for Selecting Values of Input Variables in The Analysis of Output from a Computer Code, *Technometrics*, *21* (1979), 2, pp. 239-245
[23] Li, L., *et al*., Multi-Objective Optimization of Cutting Parameters in Sculptured Parts Machining Based on Neural Network, *Journal of Intelligent Manufacturing*, *26* (2015), 5, pp. 891-898

Paper submitted: March 7, 2022
Paper revised: April 1, 2022
Paper accepted: August 11, 2022